Organic & Biomolecular Chemistry

ROYAL SOCIETY OF CHEMISTRY

PAPER

View Article Online
View Journal | View Issue

Cite this: *Org. Biomol. Chem.*, 2026, **24**, 1503

Directing chiral induction in hollow helical organic nanotubes

Indradip Mandal, Justin Vouillamoz and Andreas F. M. Kilbinger *

Received 27th November 2025,
Accepted 19th January 2026

DOI: 10.1039/d5ob01868d

rsc.li/obc

Helical aromatic oligoamides were synthesized *via* a polymerization strategy from amino acid-derived monomers to probe side-chain steric effects on helical chirality. Circular dichroism revealed tunable, reversible helicity dictated by substituent bulk. This work establishes tubular oligoamides as structurally precise yet responsive foldamers, enabling controlled chiroptical activity through targeted side-chain engineering.

A helical architecture is a hallmark of structural organization in both natural and synthetic systems,[1] enabling precise spatial arrangement of functional groups[2] and often conferring unique chiroptical properties.[3] Inspired by motifs in proteins, nucleic acids, and polysaccharides, chemists have developed foldamers, which are synthetic oligomers that adopt stable, predictable conformations and act as versatile platforms for chiral recognition,[4] catalysis,[5] molecular transport,[6] and responsive materials.[7] Among these, aromatic oligoamides have attracted sustained interest for their predictable folding, high stability, and modular synthetic design.

Tubular aromatic oligoamides developed by Gong and co-workers[8,9] form a distinct class within this family. Built from *meta*-alkoxy-linked aromatic amide units reinforced by intramolecular three-centre hydrogen bonds, these rigid backbones fold into persistent cylindrical helices with internal cavities and tunable outer surfaces. Such tubular foldamers assemble into columnar stacks *via* π–π interactions,[10] creating continuous channels for molecular encapsulation[11] or transport.[12] While structurally precise and robust, these helices have not been extensively explored for their chiroptical properties; despite their well-defined helicity, parent systems have rarely been examined for circular dichroism (CD) activity or systematic control of helical chirality.[13]

Other aromatic foldamer systems demonstrate that peripheral substituents can strongly influence helicity,[14] self-assembly,[15] and optical properties.[16] Among them, quinoline-derived oligoamides, pioneered by Huc and co-workers, have been studied extensively for helical folding,[17] chiral induction,[18] and functional group organization along a rigid aromatic helix. In such systems, remote stereocenters,[19] steric bias,[20] and hydrogen-bond-mediated conformational control have been exploited to achieve absolute helical handedness and switchable chirality in solution and the solid state.[21] Additionally, Zeng and co-workers[22] have reported macrocyclic aromatic oligomers with specific functional end groups that stack into columnar assemblies, highlighting how noncovalent forces can control supramolecular helicity. Li[23] and others[24] have designed aromatic macrocycles[25] and helices[26] bearing hydrogen-bonding and π-stacking motifs that drive hierarchical organization into nanorods, fibrils, and other anisotropic structures. These studies illustrate a general principle: the periphery of a foldamer and its side chains or appended functionalities can be as critical as the backbone in dictating folding propensity, supramolecular organization, and emergent chiral properties.[27]

In helical aromatic foldamers, side chains can influence conformation through steric effects,[28] electronic modulation of aromatic stacking, and secondary noncovalent interactions.[29] Such influences can bias helix handedness,[30] alter the helical pitch,[31] and modulate aggregation, with potential to enable reversible chiral switching.[32] However, a systematic investigation into how side-chain design affects the helicity and chiroptical signatures of "tubular" aromatic oligoamides, such as those developed by the Gong group, has not yet been reported.

Herein, we present a detailed study of side-chain-functionalized tubular aromatic foldamers that display measurable and tunable CD activity. In the absence of chiral induction, the helices typically exist as a racemic mixture of left- and right-handed forms. Incorporation of chiral side chains or chiral initiators can bias this equilibrium to favor one handedness, which is reflected in their chiroptical signals. By introducing chiral substituents of varied steric demand, we examine how peripheral modifications influence the magnitude of chiral induction. Helices bearing achiral side chains were biased toward a preferred helical sense by introducing a chiral initiating group into the backbone, exploiting the well-known 'ser-

Department of Chemistry, University of Fribourg, Chemin du Musée 9, 1700 Fribourg, Switzerland. E-mail: andreas.kilbinger@unifr.ch

geant-and-soldiers' effect. Variable-temperature CD spectroscopy reveals distinct side-chain-dependent trends, including reversible modulation of CD intensity. Structural analysis suggests these effects arise from the interplay between side-chain packing. This work demonstrates, for the first time, that Gong-type tubular foldamers can be rendered chiroptically active through targeted side-chain engineering. The resulting CD signals provide direct access to their helicity in solution, bridging the gap between structurally precise yet previously uncharacterized chiral-responsive foldamer systems.

A recently developed polymerization method[33–35] was employed by our group to synthesize oligomers and polymers directly from aromatic amino acid monomers (Fig. 1), as it can produce presumed helical foldamers in a single step. The latest phosphine-based reagent, **R** (Fig. 1), was used to activate the carboxylic acid to the corresponding acid chloride in the presence of an amine under slow monomer addition conditions (Scheme 1). Initially, monomer **A**, bearing minimally sterically demanding methoxy groups, was polymerized using the chiral initiator **I1** to yield **PA1**. Although the polymerization was targeted to form only a 16-mer (**A** : **I1** = 16 : 1), precipitation of the resulting polymer was observed. This limited the solubility and hindered subsequent characterization by size-exclusion chromatography (SEC) in DMF and *via* NMR spectroscopy. Fortunately, CD spectroscopy could be performed in both $CHCl_3$ and DMF due to the low concentration needed for the measurements. In $CHCl_3$, a positive Cotton effect was observed (Fig. 2A). Concentrations from 0.01 to 0.1 mg mL^{-1} showed a proportional increase in both CD (Fig. 2B) and absorbance intensities (Fig. 2C). Fluorescence measurements were also conducted in $CHCl_3$ (0.01 mg mL^{-1}) (Fig. 2D) using the excitation wavelength λ = 274 nm where the absorbance value was 0.1 AU (Fig. S). In DMF, a lower-intensity CD signal was detected, and heating the solution up to 110 °C caused a slight decrease in CD intensity (Fig. 2E). Upon cooling to 20 °C and equilibrating for one hour, the CD intensity recovered almost to that of a freshly prepared sample at 20 °C (Fig. 2F), indicating that heat can act as a stimulus for these chiral initiator-induced helices. To increase solubility and thereby to obtain control over the helix synthesis during polymerization, monomer **B** was prepared (see the SI) and initiated with **I1** at a **B** : **I1** ratio of 8 : 1. SEC analysis of the precipitated polymer

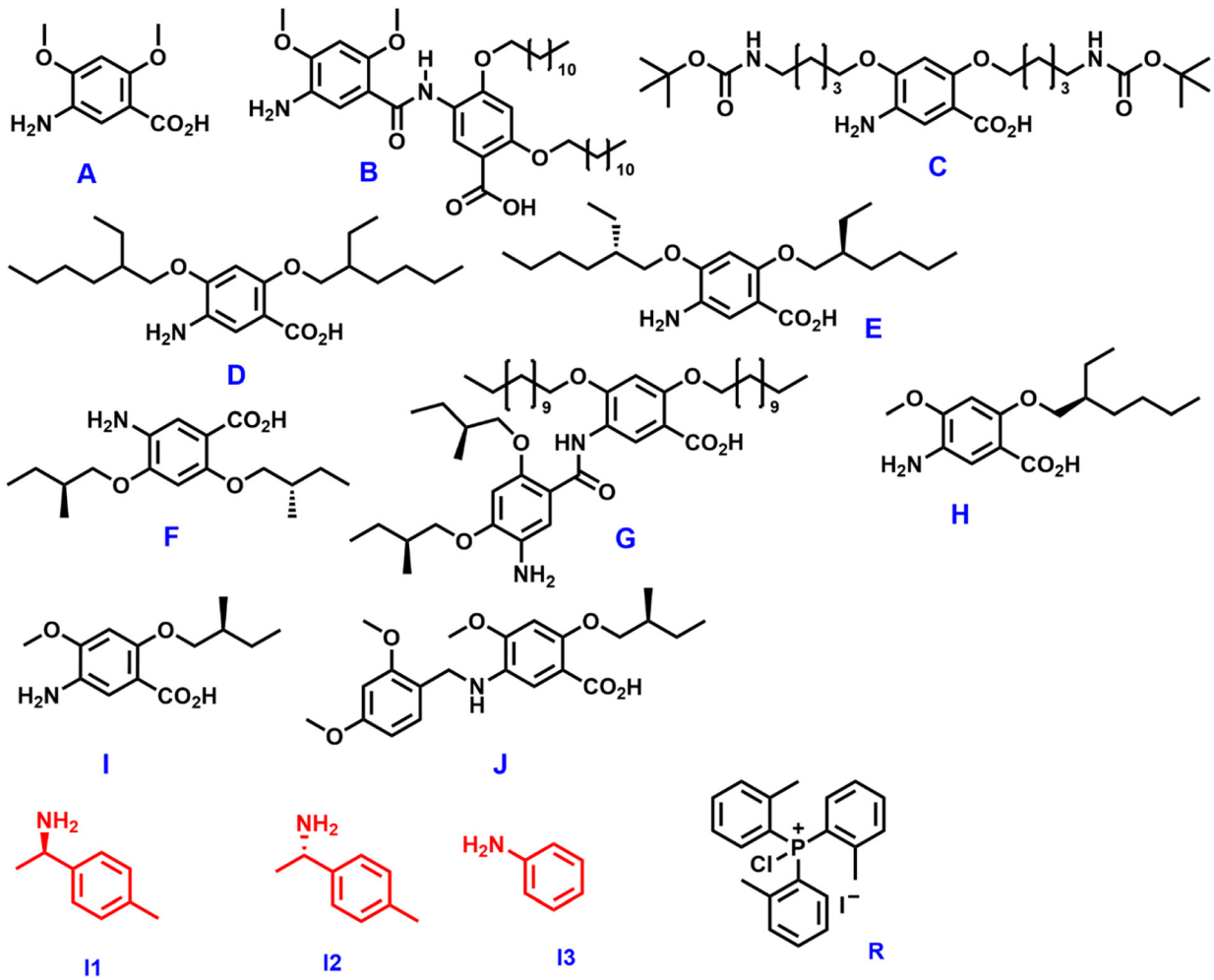

Fig. 1 Chemical structures of the monomer (**A–J**), initiators (**I1–I3**) and the phosphine reagent (**R**) used in this study.

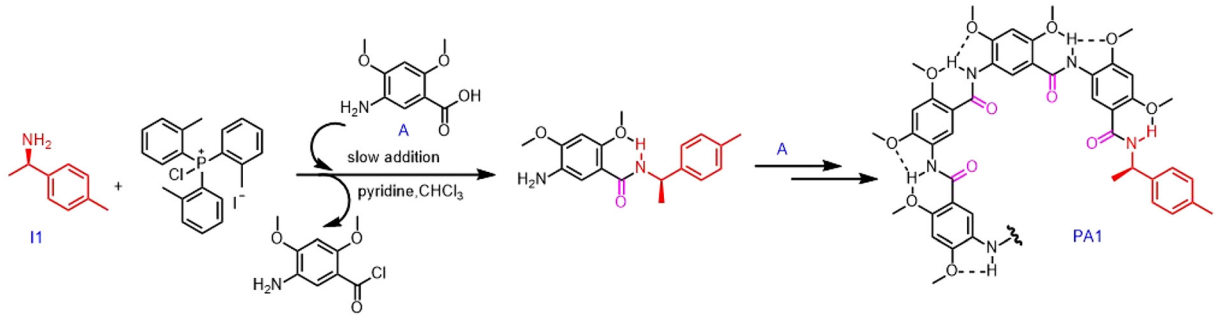

Scheme 1 The polymerization process to produce foldamers employing reagent **R**.

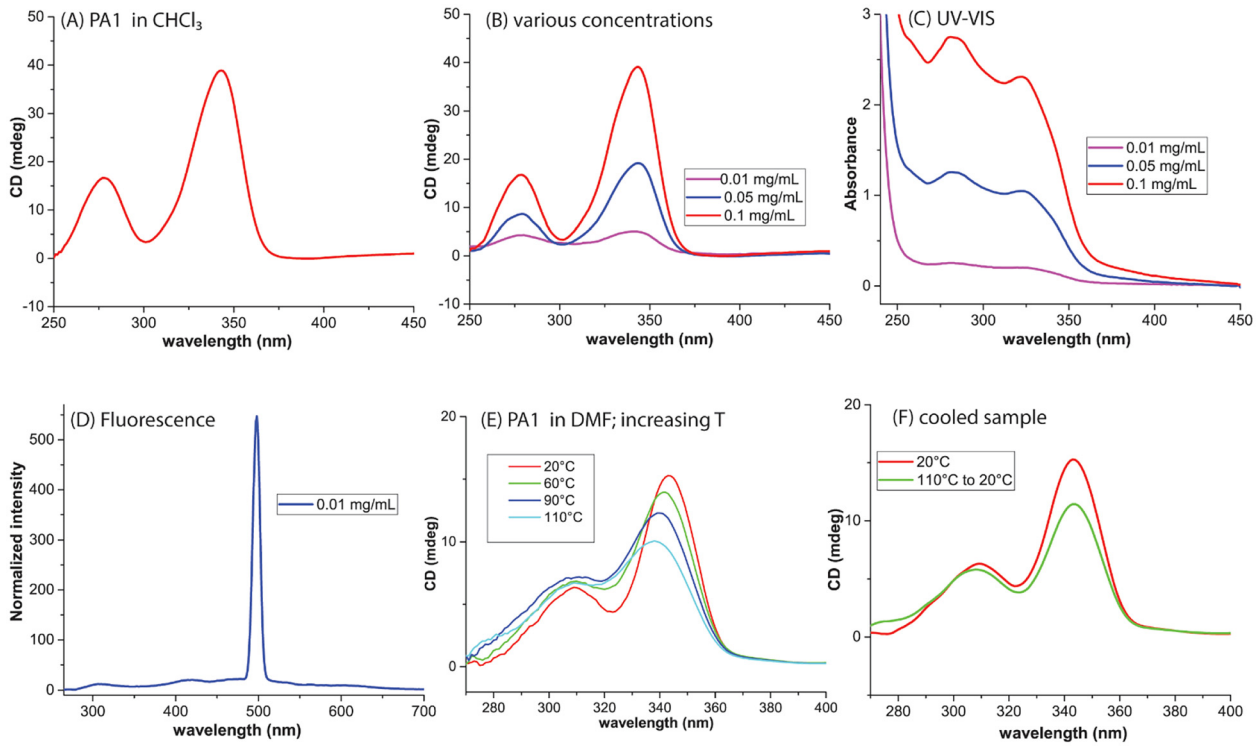

Fig. 2 Analysis of polymer **PA1**. (A) CD spectrum at 20 °C in $CHCl_3$ (0.1 mg mL^{-1}). (B) CD spectra in $CHCl_3$ at 20 °C, at varying concentrations. (C) UV-VIS spectra at 20 °C at varying concentrations. (D) Fluorescence spectrum of **PA1** in $CHCl_3$. (E) Effect of increasing temperature on the CD intensity of **PA1** in DMF (0.05 mg mL^{-1}). (F) The heated sample when cooled back to 20 °C.

PB1 (from cold methanol) in DMF showed a number-average molar mass (M_n) of 4.8 kDa (theoretical M_n = 5.3 kDa) with a dispersity of 1.09. CD spectra were recorded in a range of solvents at a fixed concentration (0.1 mg mL^{-1}), including $CHCl_3$, DMF, a $CHCl_3$/methanol (1 : 1) mixture, and CCl_4. In all cases, a positive Cotton effect was observed (Fig. 3A), though with varying intensities. $CHCl_3$ showed the highest intensity signal among the solvents tested here. Temperature-dependent CD measurements were further performed in $CHCl_3$ and DMF. Heating a chloroform solution to 40 °C did not alter the CD signal (Fig. S3) whereas increasing temperature showed a continuous decrease of the CD signal in DMF (Fig. 3B). Plotting of the CD absorption maximum (at 340 nm) *vs.* temperature yielded a cross-over point at around T = 80–85 °C which resembled a melting transition of **PB1** in DMF (Fig. 3C). When the same solution was gradually cooled to 20 °C, the CD signal returned to almost its original value indicating a reversible process (Fig. 3D). This phenomenon indicates that **PB1** is thermally stable yet dynamic. The polymer underwent reversible unfolding and refolding of its helices in response to temperature changes. This phenomenon should be similar in magnitude and transition temperature for similar helices. However, this scenario was less pronounced in the case of **PA1** compared to **PB1**. We assume that the three center hydrogen bonding strength is of similar magnitude for **PA1** and **PB1**, and in fact, all helices synthesized here. The enthalpic benefit from

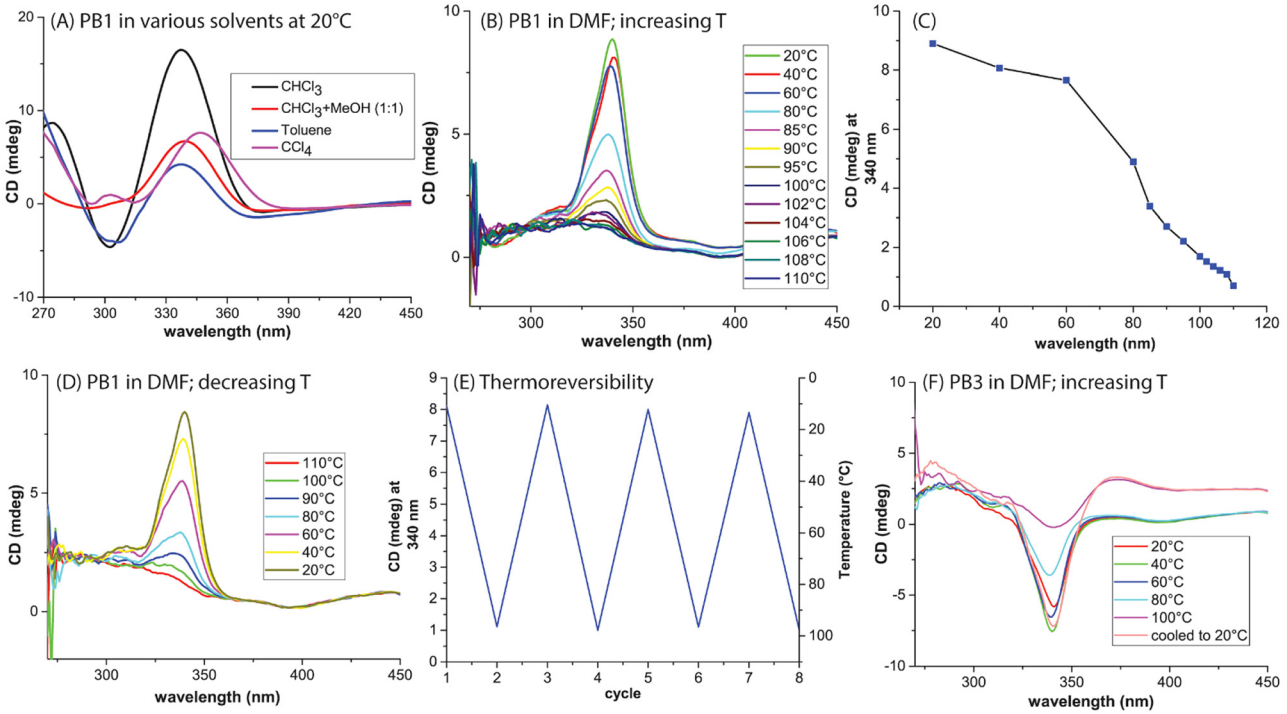

Fig. 3 (A) CD spectra of **PB1** in different solvents. (B) Effect of increasing temperature on CD signal intensities of **PB1** dissolved in DMF (0.05 mg mL^{-1}). (C) Plotting CD intensity at 340 nm *vs.* temperature yielded the melting temperature of **PB1** in DMF. (D) Effect of cooling of the heated **PB1** sample. (E) Thermoreversible helicity of **PB1** in DMF (0.05 mg mL^{-1}) under repeated heating and cooling cycles. (F) Temperature ramping effect of **PB3** in DMF (0.05 mg mL^{-1}).

π-interactions between phenyl rings of adjacent helical turns, however, will be highly dependent on the helical pitch, which will be a function of steric bulk of the attached side chains.

It is, therefore, reasonable to assume that helices carrying bulkier side chains give rise to larger helical pitches. This in turn should decrease the strength of aromatic interactions and facilitate helical racemization. For chirally initiated helices in particular, a larger pitch will reduce the steric contact between the initiator group and the first "overlapping", *i.e.* a helical monomer unit and hence weaken the chiral induction.

We, therefore, believe that the loss of the CD signal is due to a loss of chiral bias rather than proof of complete unfolding of the helix.

To understand the effect of side chain steric bulk on parameters, such as the helical pitch, we carried out simple molecular dynamics simulations using an implicit solvent model (Hawkins–Cramer–Truhlar, see the SI for details). Helices composed of 60 phenyl rings were simulated for all monomers **A–I** for 100 ns, with the last 50 ns used for averaging geometric parameters.

We calculated the helical pitches for poly-**A** (3.45 Å) and poly(B) (5.35 Å). This difference in pitch of almost 2 Å shows how polymers of these densely side-chain decorated monomer units are very susceptible to small steric effects. Therefore, assuming a larger pitch for **PB1** compared to **PA1**, we can assume that weakened aromatic interactions in **PB1** could be responsible for a more pronounced thermal response in CD-spectroscopy. To examine the effect of the helix length on helicity, **PB2** was synthesized under the same conditions as **PB1**, except using a **B** : **I1** ratio of 16 : 1. A chloroform-soluble polymer was obtained; however, **PB2** precipitated at the SEC characterization concentration (2 mg mL^{-1}) in DMF, and SEC in chloroform yielded no elution, the reason for which remains unclear. Despite these challenges, CD analysis of **PB2** revealed a Cotton effect similar to that of **PB1**, confirming the presence of helical folding in longer oligomers in solution (SI, Fig. S5). However, at the same mass concentration (0.1 mg mL^{-1}) the CD intensity of **PB2** was lower than that of **PB1**, indicating that the chiral bias does not propagate along the entire length of the helix for this type of monomer (Fig. S8). Moreover, **PB1** exhibited a thermoreversible behaviour, with CD signals decreasing upon heating and largely recovering upon cooling for several cycles, indicating reversible helical folding (Fig. 3E). Initiator **I2** was used to synthesize **PB3** (**I2** : **B** = 1 : 8), which, as expected, showed a negative Cotton effect (Fig. 3F) and a similar thermal response during CD analysis.

To improve the solubility of the helical polymers in both nonpolar ($CHCl_3$ during synthesis) and polar (DMF for SEC analysis) solvents, a pentyl *tert*-butoxycarbonyl (BOC) side group was introduced into monomer **C**. Monomer **C** was polymerized using **R** and **I1** under slow monomer addition (0.07 mL h^{-1}) conditions. The resulting 20-mer, **PC1**, exhibited controlled M_n (11 kDa) and dispersity (1.08) in SEC (DMF). Subsequently, a 50-mer, **PC2**, was synthesized with similarly

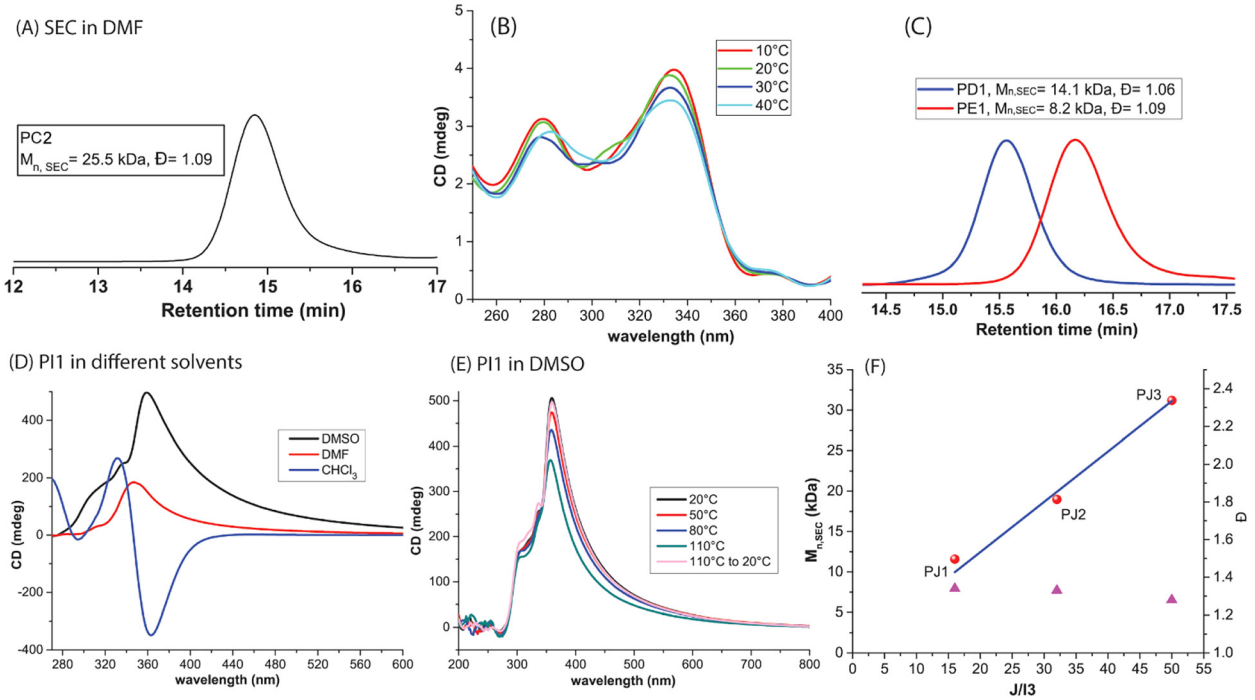

Fig. 4 (A) SEC elugram of **PC2**. (B) CD spectra of **PC2** in $CHCl_3$ (0.1 mg mL^{-1}) at various temperatures. (C) SEC elugrams of **PD1** and **PE1**. (D) CD spectra of **PI1** in different solvents (0.1 mg mL^{-1}) at 20 °C. (E) **PI1** in DMSO (0.1 mg mL^{-1}) at different temperatures. (F) Linear plot of M_n *vs.* the **J**/**I3** ratio showing control over polymerization of monomer **J**.

controlled M_n and dispersity (Fig. 4A). CD analysis of **PC2** revealed a positive Cotton effect in $CHCl_3$, although the signal intensity was comparatively weak (Fig. 4B). Heating a $CHCl_3$ solution up to 40 °C did not result in any loss of CD signals. Despite the longer chain length, the foldamer retained its helical conformation, consistent with the classical sergeant-and-soldiers effect. MD simulations of a 60mer of poly(**C**) allowed the calculation of a pitch of 4.14 Å, which was much shorter than that of polymers of **A** and **B**. MD simulations show that attractive H-bonds amongst the side chain BOC urethane groups are responsible for a more compact and less sterically interfering periphery of the helix, which manifests in a smaller pitch and hence reduced thermoresponsive behavior in CD-measurements.

To investigate the effect of steric crowding on the solution-state helicity of these foldamers, ethylhexyl side chains were introduced to afford monomers **D** and **E**. The only difference between the two monomers is that **D** is racemic, whereas **E** is the enantiomerically pure (*S*)-isomer (see the SI). Mosher's ester derivatives were prepared from the synthesized pure (*S*) alcohol and the commercial racemic alcohol to prove the enantiomeric purity of the synthesized side groups. ^{19}F and ^{13}C NMR comparison of both esters unequivocally proved that the chiral (*S*)-2-ethylhexan-1-ol was indeed enantiomerically pure (see Fig. S12–S15). Monomer **D** was polymerized using **I1** to target a 25-mer (**PD1**), which was well-characterized by SEC (Fig. 4C). As expected, **PD1** did not exhibit any CD signals in $CHCl_3$, CCl_4, or DMF. A similar observation was made for **PE1** (synthesized from **E** with **I3**, see the SI), which was striking given that each repeat unit contains two chiral side chains. MD simulations of a 60mer of poly(**E**) gave a pitch of 6.43 Å.

These results strengthen our hypothesis that steric side chain bulk affects the helical pitch, which in turn results in a loss of the ability to be chirally biased by the initiator or side chains.

Additionally, **PD1** and **PE1** showed good solubility in DMF and can be readily characterized by SEC, despite their inherent hydrophobicity. This observation aligns with our hypothesis that a larger helical pitch allows solvent molecules to interact with the exposed amide and phenyl groups, enhancing polymer solubility in DMF. In fact, the molecular dynamics simulated pitches (see the SI) can only be considered as minimum values, useful for comparing the effect of different substituents. We believe that the excellent solubility of **PD1** and **PE1** can only be explained by solvation of the helices, which would significantly expand their helical pitches if the three center H-bonds remain unbroken.

Next, a systematic study of the effect of steric groups on CD behavior was performed by designing monomers **F**–**I**. Monomer **F** has a slightly lower steric bulk than **D** and **E**; **G** contains alternating chiral branched and achiral straight alkyl groups; **H** bears a methoxy group on one side and a bulky (*S*)-configured ethylhexyl side chain on the other, whereas **I** has one methoxy group on one side and a chiral (*S*)-2-methylbutyl on the other. **F**, **G**, and **H** could all be polymerized in a controlled manner (see the SI). **PF1** (pitch: 5.80 Å, see the SI) and

PH1 (pitch: 5.10 Å, see the SI) were CD silent, whereas **PG1** (pitch: 5.27 Å, see the SI) showed a very weak CD signal in CCl_4 (Fig. S7 and S8).

Gratifyingly, **PI1** (pitch: 4.90 Å, see the SI) showed a strong CD signal across multiple solvents and temperatures, including DMSO (Fig. 4D). In $CHCl_3$, a bisignate signal was initially observed but disappeared when the solution was kept at room temperature overnight, likely due to aggregation-induced precipitation. In DMF and DMSO, **PI1** consistently showed a positive Cotton effect, with the highest intensity in DMSO. Notably, the CD signal in polar, potentially H-bond-disrupting solvents persisted for extended periods without racemization. Heating the DMSO solution to 100 °C did not alter the CD signal much (Fig. 4E), which also remained stable at room temperature for over 45 days. Interestingly, unlike **PB1**, here, the CD intensity did not decrease to almost zero upon heating in either DMSO or DMF (Fig. S9). The dissymmetry factor (*g*-factor) of **PI1** in DMSO at room temperature was calculated as 9.8×10^{-3} (see the SI). This high *g*-factor suggests significant chiral asymmetry in the electronic transitions of **PI1** in a polar solvent such as DMSO.

The monomer structures of **H** and **I** only differ slightly in that the stereogenic center in **H** carries an ethyl and a butyl group, whereas the stereogenic center of **I** carries a methyl and an ethyl group. This slight difference in the steric bulk leads to a 0.2 Å (see MD simulations) larger helical pitch for **H** (5.10) compared to **I** (4.90) and complete loss of any helical bias in **H**. It is important to note that branched side chains, which are often used for increased solubility, can easily affect the helical folding if the steric bulk due to the branching group is too close to the helical core.

Due to strong aggregation, **PI1** was insoluble for NMR or SEC analysis. To overcome this, a protection–deprotection strategy was employed. Monomer **J** was prepared in one step from **I** and polymerized to three different lengths (**PJ1**: 16-mer, **PJ2**:32-mer, and **PJ3**: 50-mer). A controlled polymerization could be achieved as shown by the linear relationship between observed M_n and monomer (**J**) to initiator (**I3**) ratio employed (Fig. 4F). As expected, **PJ1** did not show any CD signal. Following trifluoroacetic acid treatment and trituration from methanol, the resulting polymer exhibited a sharp CD signal in $CHCl_3$, confirming the pH-triggered helical folding of the polymer (Fig. S12). Fluorescence spectra of both protected and deprotected **PJ1** revealed an additional emission peak at around 420 nm, which is likely attributable to folding of the helical backbone (Fig. S13).

Conclusions

In summary, we demonstrate that the helicity and chiroptical activity of tubular aromatic oligoamide foldamers can be precisely modulated through side-chain design and chain length. Minimally sterically demanding side chains yield strong, thermoresponsive CD signals, while bulky substituents suppress the signal, highlighting the critical role of steric effects and likely the helical pitch. Notably, the introduction of optimized side chains further enables stable CD responses, even in polar solvents and at elevated temperatures. These findings were further supported by molecular dynamics simulations of polymers constructed from all monomers. These results establish Gong-type *meta*-alkoxy-linked *meta*-aminobenzamide-based tubular foldamers as a versatile platform for controlling solution-state helicity and designing chiral-responsive materials through side-chain engineering. These results also suggest that in all applications of these polymers as tube-like structures or channels, the side-chains must be designed carefully in order not to widen the helical pitch beyond the point where aromatic interactions are lost.

Author contributions

IM conceived the project. IM and JV synthesized the monomers. IM performed the polymerizations and analyses. AFMK supervised the research. All authors reviewed the manuscript.

Conflicts of interest

There are no conflicts to declare.

Data availability

The data supporting this article have been included as part of the supplementary information (SI). Supplementary information: figures, data, detailed experimental protocols and characterisation of new compounds. See DOI: https://doi.org/10.1039/d5ob01868d.

Acknowledgements

IM, JV, and AFMK thank the Department of Chemistry, University of Fribourg, Switzerland, for support.

References

1 T. Leigh and P. Fernandez-Trillo, *Nat. Rev. Chem.*, 2020, **4**, 291.
2 M. Zwillinger, P. S. Reddy, B. Wicher, P. K. Mandal, M. Csékei, L. Fischer, A. Kotschy and I. Huc, *Chem. – Eur. J.*, 2020, **26**, 17366.
3 E. Yashima, K. Maeda, H. Iida, Y. Furusho and K. Nagai, *Chem. Rev.*, 2009, **109**, 6102.
4 T. Ikai, T. Matsumoto, S. Takeda, K. Oki and E. Yashima, *Macromolecules*, 2025, **58**, 6943.
5 L. Zhou, K. He, N. Liu and Z.-Q. Wu, *Polym. Chem.*, 2022, **13**, 3967.
6 S. Farooq, J. A. Malla, M. Nedyalkova, R. V. M. Freire, I. Mandal, A. Crochet, S. Salentinig, M. Lattuada,

C. T. McTernan and A. F. M. Kilbinger, *Angew. Chem., Int. Ed.*, 2025, **64**, e202504170.
7 M. Lago-Silva, M. Fernández-Míguez, R. Rodríguez, E. Quiñoá and F. Freire, *Chem. Soc. Rev.*, 2024, **53**, 793.
8 B. Gong, *Acc. Chem. Res.*, 2008, **41**, 1376.
9 T. A. Sobiech, Y. Zhong and B. Gong, *Org. Biomol. Chem.*, 2022, **20**, 6962.
10 X. Wei, G. Zhang, Y. Shen, Y. Zhong, R. Liu, N. Yang, F. Y. Al-mkhaizim, M. A. Kline, L. He, M. Li, Z.-L. Lu, Z. Shao and B. Gong, *J. Am. Chem. Soc.*, 2016, **138**, 2749.
11 Y. Zhong, T. A. Sobiech, B. Kauffmann, B. Song, X. Li, Y. Ferrand, I. Huc and B. Gong, *Chem. Sci.*, 2023, **14**, 4759.
12 A. J. Helsel, A. L. Brown, K. Yamato, W. Feng, L. Yuan, A. J. Clements, S. V. Harding, G. Szabo, Z. Shao and B. Gong, *J. Am. Chem. Soc.*, 2008, **130**, 15784.
13 J. Cao, M. Kline, Z. Chen, B. Luan, M. Lv, W. Zhang, C. Lian, Q. Wang, Q. Huang, X. Wei, J. Deng, J. Zhu and B. Gong, *Chem. Commun.*, 2012, **48**, 11112.
14 K. Kuyama, F. Takeda, A. Ikeda, K. Tanaka, K. Katagiri, M. Kawahata, Y. Okada, N. Kobayashi, H. Kagechika and A. Tanatani, *Org. Biomol. Chem.*, 2025, **23**, 4927.
15 Z. Pang, T. Qi and B. Li, *Org. Biomol. Chem.*, 2021, **19**, 5555.
16 V. Laffilé, K. Moreno, E. Merlet, N. McClenaghan, Y. Ferrand and C. Olivier, *Org. Biomol. Chem.*, 2023, **21**, 3644.
17 S. Wang, J. Sigl, L. Allmendinger, V. Maurizot and I. Huc, *Chem. Sci.*, 2025, **16**, 1136.
18 H. Jiang, C. Dolain, J.-M. Léger, H. Gornitzka and I. Huc, *J. Am. Chem. Soc.*, 2004, **126**, 1034.
19 V. Maurizot, C. Dolain and I. Huc, *Eur. J. Org. Chem.*, 2005, **2005**, 1293.
20 A. M. Kendhale, L. Poniman, Z. Dong, K. Laxmi-Reddy, B. Kauffmann, Y. Ferrand and I. Huc, *J. Org. Chem.*, 2011, **76**, 195.
21 T. Qi, V. Maurizot, H. Noguchi, T. Charoenraks, B. Kauffmann, M. Takafuji, H. Ihara and I. Huc, *Chem. Commun.*, 2012, **48**, 6337.
22 H. Zhao, W. Q. Ong, F. Zhou, X. Fang, X. Chen, S. F. Y. Li, H. Su, N.-J. Cho and H. Zeng, *Chem. Sci.*, 2012, **3**, 2042.
23 D. Zhang, W. Wang and Z. Li, *Chem. Rec.*, 2015, **15**, 233.
24 K. Kreger, F. Behrendt and J. C. Brendel, *J. Polym. Sci.*, 2025, **63**, 4450–4465.
25 C. Ren, V. Maurizot, H. Zhao, J. Shen, F. Zhou, W. Q. Ong, Z. Du, K. Zhang, H. Su and H. Zeng, *J. Am. Chem. Soc.*, 2011, **133**, 13930.
26 S. Koppireddi, C.-Z. Liu, H. Wang, D.-W. Zhang and Z.-T. Li, *CrystEngComm*, 2019, **21**, 2626.
27 T. Ikai, K. Nakamura, K. Mizumoto, K. Oki and E. Yashima, *Angew. Chem., Int. Ed.*, 2023, **62**, e202301127.
28 A. Tanatani, A. Yokoyama, I. Azumaya, Y. Takakura, C. Mitsui, M. Shiro, M. Uchiyama, A. Muranaka, N. Kobayashi and T. Yokozawa, *J. Am. Chem. Soc.*, 2005, **127**, 8553.
29 S. E. Miller, A. M. Watkins, N. R. Kallenbach and P. S. Arora, *Proc. Natl. Acad. Sci. U. S. A.*, 2014, **111**, 6636.
30 T. Ikai, Y. Morita, T. Majima, S. Takeda, R. Ishidate, K. Oki, N. Suzuki, H. Ohtani, H. Aoi, K. Maeda, K. Okoshi and E. Yashima, *J. Am. Chem. Soc.*, 2023, **145**, 24862.
31 A. Yokoyama, T. Saiki, H. Masu, I. Azumaya and T. Yokozawa, *Polymer*, 2018, **134**, 175.
32 S. Kobayashi, K. Morino and E. Yashima, *Chem. Commun.*, 2007, 2351.
33 S. Pal, D. P. T. Nguyen, A. Molliet, M. Alizadeh, A. Crochet, R. D. Ortuso, A. Petri-Fink and A. F. M. Kilbinger, *Nat. Chem.*, 2021, **13**, 705.
34 S. Pal, L. Hong, R. V. M. Freire, S. Farooq, S. Salentinig and A. F. M. Kilbinger, *Macromolecules*, 2023, **56**, 7984.
35 D. P. T. Nguyen, S. Farooq, N. Meyer and A. F. M. Kilbinger, *Polym. Chem.*, 2025, **16**, 2639.